Construction and Building Materials 409 (2023) 133853

Contents lists available at ScienceDirect

Construction and Building Materials

journal homepage: www.elsevier.com/locate/conbuildmat

Experimental and analytical evaluation of the tension capacity of edgewise connected glued-in rods in mass ply panels

Tanner Field [a], Andre R. Barbosa [a,*], Reid B. Zimmerman [b], Steve Pryor [c], Arijit Sinha [a], Christopher Higgins [a]

[a] Oregon State University, USA
[b] KPFF Consulting Engineers, USA
[c] Advanced Research and Development, Simpson Strong-Tie, USA

ARTICLE INFO

Keywords:
Glued-in Rod
Mass-Ply Panel
Tension Capacity
Splice Connection

ABSTRACT

The length of mass timber wall panels is a limiting factor in designing taller buildings. Splice designs are needed to maintain panel transportability while transferring shear and moment forces from higher floors to the foundation under lateral loading. One such splice design utilizes structural adhesive to glue threaded steel rods into the ends of wall panels being connected. This paper reports tests of the tension capacity of glued-in rods embedded in Mass Ply Panels (MPP). Twenty glued-in rods were tested under monotonic and cyclic protocols. Embedment depths ranged between 304.8 mm (12 in.) and 812.8 mm (32 in.). Load and displacement were measured during tests to report values per ISO 6891 and an international code council acceptance criteria document. Elastic stiffness, peak capacity, design capacity, and a predictive capacity equation were determined. Results showed a similar stiffness for all embedment depths and a negligible difference between peak capacities from monotonic and cyclic testing. While the data reported is only directly applicable for analysis of the specific MPP and epoxy combination used in the test program, the methodology herein can be utilized for future testing of timber-adhesive glued-in rods.

1. Introduction

Glued-in rods (GIRs) provide a unique solution for hold-downs and splice connections for mass timber shear walls. Many designs require strapping to be nailed to the exterior of the wall panel, but GIRs allow this connection to be hidden, preserving the panel aesthetics. Additionally, the use of embedded steel rods provides corrosion resistance to the connection and potential fire resistance compared to exposed connections as mentioned in the introduction of several publications [2,3,4,6,8,9]. While there are many advantages to the connection, during fabrication of specimens for testing, disadvantages to the connection were foreseeable. These include more challenging construction tolerances and fit up, inspection, and repair compared to external methods as well as wait-times associated with adhesive curing. In addition to wait-time, there is also potential for improper mixing and curing of the adhesive or improper placement with partial filling of the hole by the adhesive. These conditions can reduce the ultimate tensile capacity of the connection, but they can be mitigated through careful construction practices and inspection.

Previous tests have established that several factors affect the capacity of GIR connections, including rod diameter, materials (timber, adhesive, and rod material), connection geometry, and installation process [2,10,7,8]. Embedment depth and edge distance have a significant effect on the ultimate tensile capacity of the connection [11,12,13,10,15,16]. Deng [11] provides comprehensive research on glued-in rods in glulam timber elements. Testing of deformed versus threaded bars concluded that threaded bars resist approximately 20 % higher peak loads, informing the decision to use threaded bars. Additionally, tests of different structural adhesive combinations (Araldite K-80 structural grout, West System Z105, and Z205/Z206 hardener, Araldite 2005) in radiata pine glulam led to the conclusion that each timber-adhesive combination produces unique outcomes.

Table 1 introduces several predictive equations on the ultimate tensile capacity of GIR connections available the literature. Other equations exist but are variations many can be considered variations of the ones presented in the Eurocode 5. These existing equations are

* Corresponding author at: Corvallis, OR 97331, USA.
E-mail address: andre.barbosa@oregonstate.edu (A.R. Barbosa).

https://doi.org/10.1016/j.conbuildmat.2023.133853
Received 17 June 2023; Received in revised form 6 September 2023; Accepted 16 October 2023
Available online 29 October 2023

summarized in Tlustochowicz et al. [2], Stepanic et al. [17], and Wiberg [18]. However, minimal changes have been made to the predictive equations for GIR since the work of Tlustochowicz et al. [2]. Based on the large number of tests and variables tested, Deng [11] presented a predictive capacity equation for the ultimate tensile load of the connection that utilizes the basic geometry of the connection: diameter of the bar, length of embedment depth, edge distance, and hole diameter; and three calibrated factors: epoxy factor, bar type factor, and moisture content factor (k_b,k_e,k_m). Deng's [11] equation is significantly different from the European code equations, which typically rely on the density of the timber and the shear strength of the adhesive. Despite significant research into GIRs beginning in the 1990 s, research has not produced consensus upon a design equation utilizing these parameters, evident by the similar equations and conclusions found in studies by Tlustochowicz et al. [2] in 2010 and Zhang et al. [8] in 2022. Therefore, equations that most reasonably predict strength with respect to the most influential parameters in the equation should be utilized, allowing for the calibration of each timber, adhesive, and rod combination.

Serrano et al. [12] developed an equation that utilizes shear strength of adhesive, axial stiffness of adhesive, α factors, and β factors, among other geometric values. While this equation provides a considerable number of factors, it also requires multiple steps for calculation. Chans et al. [13] utilizes a shear strength value of the joint for a specific slenderness ratio of the rod alongside the density of wood, embedment depth, and rod diameter. While the use of wood density is desirable, the equation is based on the shear strength for a slenderness (λ) of 10 and then is corrected for specific connection variations. Steiger et al. [10] reported on similar tests reported in Deng [11] for different structural adhesives. Steiger et al. [10] highlighted that some adhesives were shown to be more effective than others, but it is unknown how different adhesives will work with varied species and engineered wood types. Ayansola et al. [16] highlighted that exploring additional adhesives would be important for GIR connections. Azinovic et al. [4] and Ayansola et al. [16] tested GIR connections in cross-laminated timber (CLT) panels. They determined that while the data has similarities with other literature, each CLT panel test could exhibit different load responses based on if rods are placed between plys or within a single ply and variability across samples. The observed variability in responses further increases the need for testing for each combination affecting the tensile capacity [2,8].

Suggested values for edge distance vary across the literature. They are not comparable due to differences in timber species or layup between tests. Still, there appears to be agreement that a minimum edge distance of 2.5d, where d is the diameter of the rod, is acceptable [2,19,20,17,21,22,7,8,23]. While some studies use both bigger and smaller values, Thamboo et al. [23] performed a reliability analysis using an available testing database. They found that all the prior studies provided the minimum 2.5d edge distance.

There is agreement that embedment depth has a nonlinear relationship with tensile capacity and is the most influential parameter in predicting the ultimate tensile capacity of the connection [2,13,15,5,8]. Additionally, tensile capacity versus embedment depth typically follows a calibrated power law. The embedment depth is present in all design equations but, in some cases, is shown as a slenderness ratio of the rod, λ, defined as the ratio of embedment depth to the rod diameter.

While most available tests, including this work, are performed on single rods, the tensile capacity of a single rod is not enough for many applications, requiring research on multiple rod effects. Tlustochowicz et al. [2] found minimal work in their state-of-the-art review on multiple rod connections, but all work concluded that consideration must be given to the force distribution of this type of connection. For example, a brittle failure of a single rod due to nonuniform force distribution may cause overall failure of the joint. Gonzalez et al. [3] performed work on multiple GIRs but did not conclude on the difference between single and multiple GIR connections. However, Thamboo et al. [23] confirms that "the resistance of multiple GIR connections can be less than that predicted from a single GIR connection due to the grouping effect." Xu et al. [22] recently proposed an equation for the effective number of rods, which is given by:

$$n_{ef} = 0.193n^{0.892} \bullet d^{0.390} \bullet \lambda^{0.136} \bullet \left(\frac{a}{d}\right)^{0.164} \quad (5)$$

where n is the number of rods, d is the diameter of the rods, λ is the slenderness ratio taken as the ratio of embedment depth to the rod diameter, and a is the rod spacing. Ultimately, before further work on multiple GIRs is relevant, a cohesive design equation is required for single GIRs.

Mass plywood panels (MPPs) are an engineered veneer mass timber product constructed with specific orientation requirements that provide a strong and weak axis direction of the panel. MPP differs from

Table 1
Summary of equations for tension capacity.

Reference	Equation(s)	Eqn. No.	Wood Species and (or) Type	Adhesive Type	Number of Tests
[11]	$F = 10.94 \bullet k_b \bullet k_e \bullet k_m \left(\frac{l}{d}\right)^{0.86} \left(\frac{d}{20mm}\right)^{1.62} \left(\frac{h}{d}\right)^{0.5} \left(\frac{e}{d}\right)^{0.5}$	(1)	Pine Glulam	K-80, West System, Araldite 2005	128
[12]	$P_u = \tau_f \varphi_r \pi l_g \bullet \frac{(1+\alpha)sinh\beta}{\beta((\alpha+cosh\beta)cosh\beta - \sinh^2\beta)}$ where: $\beta = \sqrt{\frac{1+\alpha}{2}} \bullet \sqrt{\frac{l_g^2 \tau_f^2 \varphi_r \pi}{(EA)_w G_f}}$; $\alpha = \frac{(EA)_w}{(EA)_r} > 1$	(2)	Glulam	Fiber-Reinforced Phenol-Resorcinol, 2 Component Polyurethane, and Epoxy	N/A
[13]	$F_k = \left(0.6\rho_k^x \left(1 - \frac{0.7\left(\frac{L}{d} - 10\right)^3}{\rho_k + \left(\frac{L}{d} - 10\right)^2}\right)\right) \pi d L$	(3)	Spruce and Eucalyptus Glulam	Epoxy Resin (Hilti HIT-RE 500)	10
[14]	$P_f = \pi \bullet \tau_f \bullet h \bullet l$	(4)	Glulam, CLT, LVL, Solid Sawn	N/A	N/A

Eqn. (1): F = ultimate tensile load (kN); 10.94 constant (kN); k_m= moisture content factor; k_e= epoxy type factor;k_b = bar type factor; l=embedment length (mm); d=steel bar diameter (mm);h = hole diameter (mm); e=edge distance from center of steel bar (mm).
Eqn. (2): P_u = ultimate pullout load (kN);τ_f = shear strength of adhesive layer (N/mm2); φ_r = rod diameter; l_g=glued-in length; α=axial stiffness ratio of the rod and timber surfaces being glued; $(EA)_w$=Young's modulus in axial direction times area of wood; $(EA)_r$=Young's modulus in axial direction times area of bar; G_f = fracture energy (J/m^2).
Eqn. (3): F_k=pullout force (N); L = embedment depth (mm); d = diameter of hole (mm); ρ_k = characteristic density of wood (kg/m^3).
Eqn. (4): P_f = Pullout capacity (kN);τ_f = shear strength of adhesive (kN/mm^2); h = hole diameter (mm); l = anchorage length (mm).

laminated veneer lumber (LVL) because of seven one direction veneers and two cross-oriented veneers in MPP layup per 25 mm laminations versus the one-directional veneers in LVL. Additionally, even though MPP is classified as CLT per ANSI/PRG 320, MPP uses veneers versus larger, solid sawn, lumber used in typical CLT products.

Existing research studies span a wide variety of engineered wood products (EWPs) and wood species. Synthesis of previous studies highlights the complexity of the problem that is exacerbated by use of distinct species, adhesives, and EWPs in real-world applications. Currently, there is no approach capable of accurately accounting for the different mechanical properties of the various combinations of timber products, including species and layup, such as CLT, LVL, or MPP. Additional contributions are thus necessary to characterize the mechanical properties of each combination. The reliability analysis of current equations and available data performed by Stepinac et al. [17], Thamboo et al. [23], and Wiberg [18] show that all current equations are inconsistent and unreliable, either under or over-predicting tensile capacity alongside a large variability. Again, utilizing design equations with factors that can be calibrated for each combination of a complex GIR connection may prove to be a more effective method for reliably predicting tensile capacity.

This paper presents a novel study on the characterization of GIR embedded in MPP based on a specific experimental testing program. The experimental program consisted of testing threaded high-strength rods glued into MPP under monotonic and cyclic loading protocols at different embedment depths. Other geometric properties were held constant to develop an analytical predictive equation for the ultimate tension capacity of GIRs. While this equation includes multiple variables that were held constant for this case, embedment depth of the GIR was varied to support future designs that make use of this combination of GIR, adhesive, and MPP. Additionally, an examination of observed failure conditions is presented.

2. Materials and methods

2.1. Specimen fabrication

The MPP panels were manufactured by Freres Engineered Wood, Inc. in Lyons, OR, cut to size at Emmerson Lab at Oregon State University (OSU), then shipped to Timberlab in Portland, OR for GIR installation and panel assembly. Specimens were then delivered back to OSU for testing. The GIR installation procedure was identical for all panels.

Four (4), 101.6 mm (4 in.), F16 grade, MPP with nominal dimensions of 1066.8 mm × 2387.6 mm (42 in. × 94 in.) were fabricated. As shown in Fig. 1, each panel had eight 25.4 mm (1 in.) diameter ASTM F1554 Grade 105 steel threaded rods installed, although not all rods were tested. Rod size and type were chosen to induce failure of the adhesive-rod or adhesive-timber interface and avoid inelastic behavior of the rod. Two of these rods were embedded to a depth of 812.8 mm (32 in.). The remaining 30 were equally distributed between embedment depths of 304.8 mm (12 in.), 508.0 mm (20 in.), and 609.6 mm (24 in.). Even though 30 additional GIR were installed in case the coefficient of variations of the peak forces were large, only 20 rods were tested as detailed below.

Each rod was placed down the centerline of the panel, 50.8 mm from the long edge to the centerline of the rod, parallel to the strong axis of the MPP panel. In the perpendicular direction, the rods were nominally spaced 279.4 mm (11 in.) on-center, while the rods at either end of the panel were inserted 215.9 mm (8–1/2 in.) from the edge.

Two 8.0 mm (0.315 in.) diameter by 120.7 mm (4–3/4 in.) long Simpson Strong-Tie SDCF Timber CF screws were installed between each embedded rod. Screws were placed in two rows and alternated the direction of insertion so that each set of two screws were installed on opposite sides of the MPP. Screws were added to mitigate splitting of the panels before the ultimate tensile capacity of the connection was achieved.

A multi-step process was developed for administering adhesive into the GIR connection because proper adherence of the adhesive to both timber and rod is necessary for more uniform tensile capacity outcomes [2,17,18]. First, before applying any adhesive, 31.8 mm (1–1/4 in.) holes were prepared with a drill bit and then cleaned using a round wire brush and compressed air to remove any free particles. In addition, 9.5 mm (3/8 in.) diameter holes were drilled 25.4 mm (1 in.) from the bottom and top of each end of the 31.8 mm holes to inject the adhesive from the bottom (filler) hole and allow flow out from the top (weep) hole. Second, a small amount of adhesive was applied to the hole to fill any voids in the mass ply panel and develop a better bonding surface; a custom-designed drill "spreader" attachment was used to evenly spread the adhesive to the wall of the hole. This was accomplished by plunging the "spreader" attachment on the end of a long drill rod into the small amount of adhesive at the bottom of the hole and then slowly extracting, while simultaneously spinning, the "spreader." This first coat of adhesive was then left to cure. Third, once the first coat of adhesive had cured, the threaded rods were placed into the holes and adhesive applied through the filler holes. This method of forcing the adhesive into the bottom of the hole and allowing it to flow to the top opening avoids formation and entrapment of air bubbles along the bonded length. The adhesive used in this study was Simpson Strong-Tie CI-GV epoxy gel.

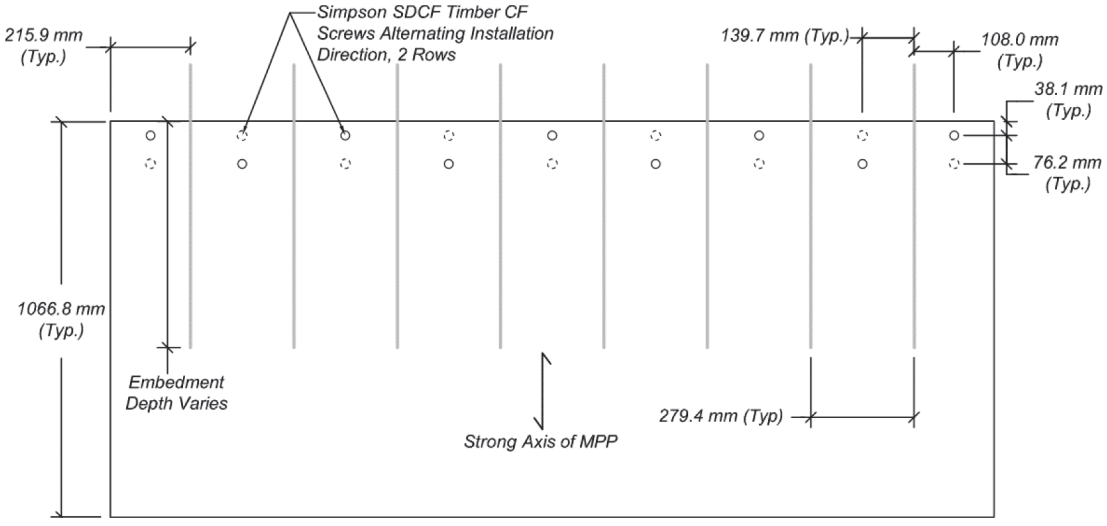

Fig. 1. Structural drawing of Mass-ply Panel with glued-in rods.

2.2. Test setup and instrumentation

Fig. 3 shows the configuration adopted for testing. Four (4) 38.1 mm (1–1/2 in.) diameter steel rods were used to connect two (2) steel HSS and anchor plates to the laboratory strong floor as shown in Fig. 3 (a) and (b). The HSS restricts upward lift of the panel during load application. A new testing fixture was developed, consisting of two (2), 50.8 mm (2 in.) thick steel plates, and four, 25.4 mm (1 in.) diameter by 152.4 mm (6 in.) steel rods. Rods were welded 25.4 mm (1 in.) offset from the center point of each edge of the plates. Fig. 2 shows diagrams of the testing jig developed for these test specimens. The upper steel plate had four holes drilled to match the layout of the actuator knuckle, and the bottom plate had one centered hole drilled to connect to the threaded rod being tested. Four (4) steel plates and two (2) HSS5x5x3/8 connected the MPP panel to the strong floor. Two (2) plates were top bearing plates, called out in Fig. 3 (c) and (d), and are 254 mm by 127 mm (10 in. by 5 in.) with 25.4 mm (1 in.) diameter holes placed 50.8 mm (2 in.) offset from the edge of both short sides of the plate. The bottom bearing plates, called out in Fig. 3 (c) and (d), are 103.2 mm × 127 mm (4–1/16 in. by 5 in.). These plates are necessary to avoid bending the HSS during testing. All connections were tightened before testing to minimize slip outside the testing region. The sample being tested was connected to the loading fixture with a washer and two (2) nuts.

The actuator load and actuator displacement were measured. Additionally, four (4) external linear variable differential transformers (LVDTs) were used to measure displacement during loading, where two (2) external LVDTs had 6.35 mm (1/4 in.) stroke, and two (2) had 25.4 mm (1 in.) stroke, which were placed on either side of the panel as indicated in Fig. 4. The resulting data showed that both LVDT lengths are acceptable due to the small deformations produced by the connection.

2.3. Testing protocols

The monotonic [1] loading protocol shown in Fig. 5a was used, where the typical elapsed testing time of 8 min was observed. For the first test performed, an estimate of the tensile capacity of the specific connection geometry was determined with Deng's equation in Table 1 using assumed factors ($k_b = 1, k_e = 1, k_m = 1$ for the initial estimate), this value was assigned as F_{est}. After the first test, future F_{est} estimates were adjusted according to this first result. For cyclic loading, the force-controlled CUREE protocol [24] shown in Fig. 5b was used, with a modification that the compression portion of testing was removed, where the typical elapsed time for each cyclic test was approximately 24 min. The compression portion of the CUREE protocol was removed since it is assumed that compression would be resisted primarily by the panel-to-panel end (i.e., wood-to-wood) bearing rather than through the GIRs. Values used for Q_0 were the experimental tensile capacity from the first monotonic test for each embedment depth. Table 2 shows a summary of samples tested under each loading protocol. Only one 812.8 mm (32 in.) specimen was tested under each monotonic and cyclic load protocol to provide a preliminary estimate on the ultimate tensile capacity. Since only one test was performed for this group, the results are shared to show this should be seen as a first step to a future robust testing program on the topic. During tests, the average moisture content of all panels was 9.9 % (COV = 5.5 %). The moisture content was measured using a Delmhorst Navigator Pro Moisture Mapping Meter set to Douglas Fir. Displacement rates for each test were determined using an estimated peak force and the time desired to reach that force. Table 3 summarizes the displacement rate used for each embedment depth. Both monotonic and cyclic tests used the same displacement rates.

2.4. Data reporting

Experimental results are first reported according to ISO 6891 [1], including peak load, displacement at peak load, initial slip, modified initial slip, and unloading and reloading elastic stiffness. Labels in Fig. 5a show notable points that are used to define the reported parameters.

The initial slip is the displacement of the rod at the loaded end during the first loading phase at 40 % of peak load, v_{04}. Per ISO 6891 [1] the modified initial slip is given by:

$$v_{i,mod} = \frac{4}{3}(v_{04} - v_{01}) \tag{6}$$

where, v_{04} and v_{01} are the displacements of the rod during the first loading phase at 40 % and 10 % of the peak load, respectively, where these points are illustrated in Fig. 5a.

The elastic modulus of the unloading phase is given by:

$$E_{unload} = \left|\frac{F_{14} - F_{11}}{v_{14} - v_{11}}\right| \tag{7}$$

where, F_{14} and F_{11} are the loads applied at the extreme ends of the unloading phase, and v_{14} and v_{11} are the respective displacements at these loads.

The elastic modulus during the reloading phase is given by:

$$E_{reload} = \left|\frac{F_{21} - F_{24}}{v_{21} - v_{24}}\right| \tag{8}$$

where, F_{21} and F_{24} are the loads applied during the elastic portion of the final reloading phase (10 % and 40 % of peak load, respectively) and v_{21} and v_{24} are the respective displacements at these loads.

For the cyclic tests, peak load, and cyclic elastic stiffness are reported. The cyclic elastic stiffness is the mean of the calculated stiffness during the three loading phases highlighted in red in Fig. 5b.

Experimental results are also summarized according to GIR acceptance criteria ICC-AC526. The reported parameters in this case are:

(1) Nominal glued-in rod (GIR) strength is the average peak load for three (3) monotonic tests at each embedment depth.

Fig. 2. (a) Elevation of Custom Testing Jig and (b) Isometric Rendering.

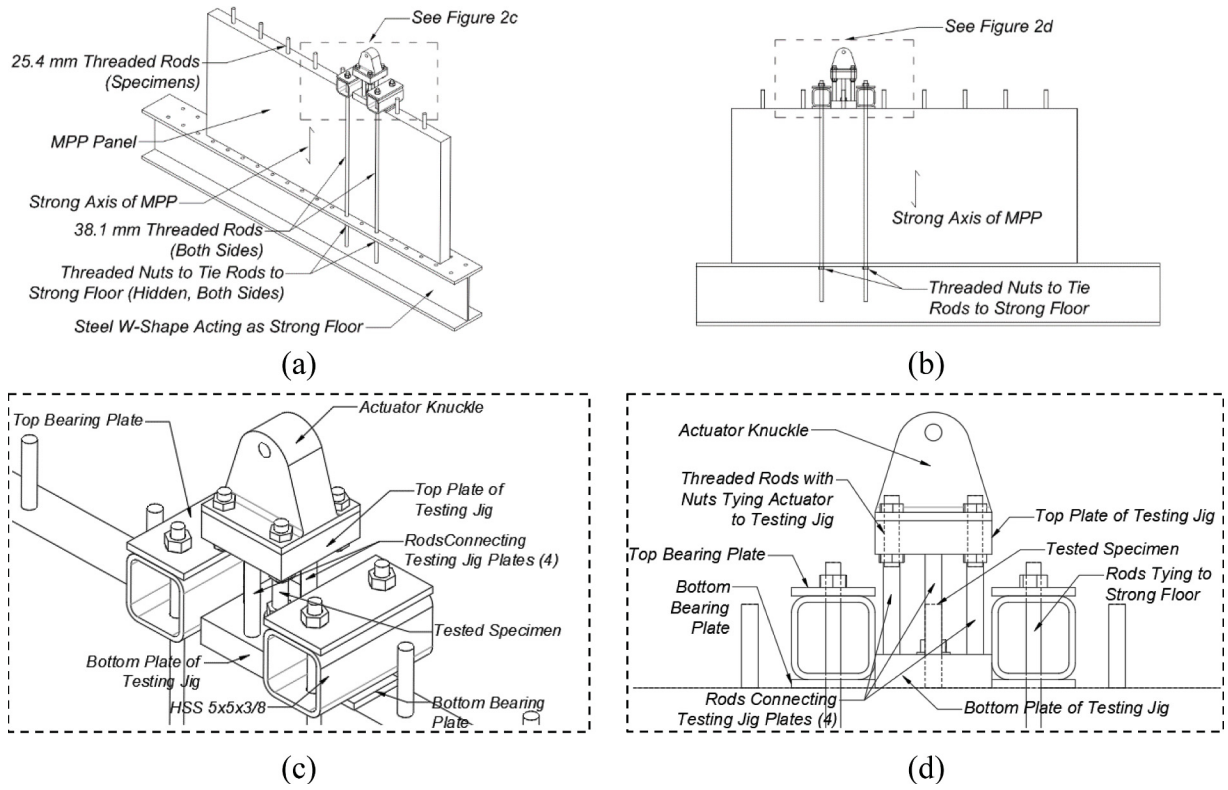

Fig. 3. Diagram of Testing Configuration, (a) isometric rendering, (b) elevation view, (c) close-up of assembly, and (d) close-up elevation view.

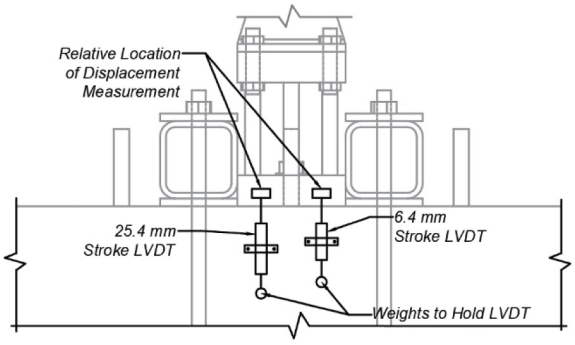

Fig. 4. View of the front face of the panel with indicative locations of two LVDTs. Identical sensors were installed on the back face of the panel.

(2) Allowable GIR strength is the nominal strength divided by a factor of safety of five (5).
(3) LRFD GIR strength, determined by applying a format conversion factor, K_F, of 3.32, a resistance factor, φ, of 0.65, and a time effect

Table 2
Test matrix including embedment depth and loading protocol.

Embedment Depth	Loading Protocol	Number of Tested Specimens
304.8 mm	Monotonic	3
	Cyclic	3
508 mm	Monotonic	3
	Cyclic	3
609.6 mm	Monotonic	3
	Cyclic	3
812.8 mm	Monotonic	1
	Cyclic	1
Total		20

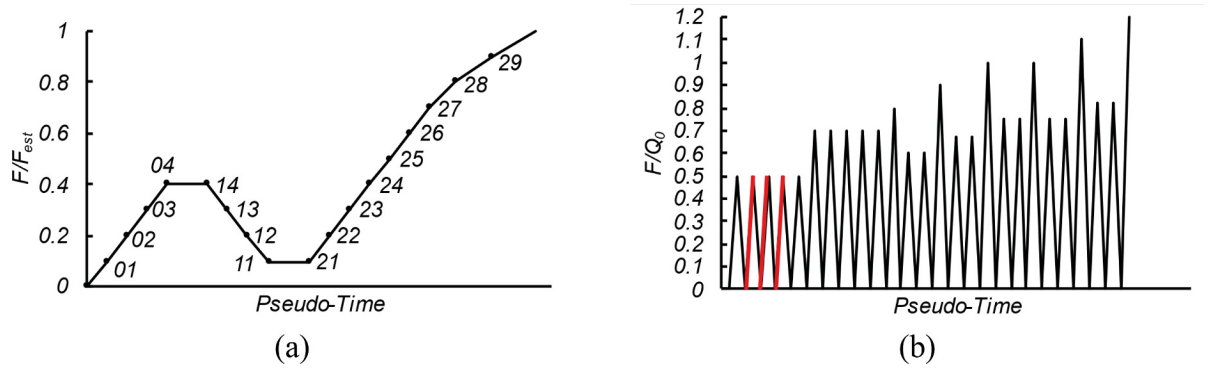

Fig. 5. Loading protocols used in study: (a) ISO 6891 [1] with F_{est} estimated with Deng equation from Table 1, and (b) Tension-only version of the force-controlled CUREE protocol used for cyclic testing with Q_0 the peak load of the first monotonic test for each embedment depth. Loading phases used for cyclic elastic stiffness calculations are highlighted in red.

Table 3
Actuator displacement rate for each embedment depth.

Embedment Depth (mm)	Displacement Rate (mm/min)
304.8	0.549
508.0	1.524
609.6	1.905
812.8	2.057

factor, λ, of 1.0 to the allowable GIR strength. Values were determined following Table N3.3 in Appendix N of the 2018 National Design Specification (NDS) for Wood Construction.

(4) Displacement at nominal and allowable GIR strength, determined as the average displacement of monotonic tests at failure and the displacement at allowable load, respectively. Values were determined by subtracting the average initial slip defined in ISO 6891 [1] for each embedment depth from displacement at peak and allowable loads, respectively.

(5) Displacement limit defined in ICC-AC526.

3. Results

Fig. 6 shows a representative graph of monotonic and cyclic test load versus displacement test results. From the figure, it is apparent that the upper envelope of each curve is similar when reporting data for the two (2) LVDTs. From zero load to 67 % of peak load, the load–displacement curve shows a linear stiffness, and from 67 % peak load to failure, stiffness degrades until failure, with the final 10 % of peak displacement showing nearly zero increase in force. However, the first 10 kN (2.25 kips) of load displays an initial loading phase that begins with minimal load gain relative to displacement, correlating to the testing system and specimen taking up slack in the load train prior to significant loading. Loud "popping" sounds were heard at failure and concurrently a steep drop in load (not shown) was observed. Note that the data shown are for two (2) 508.0 mm (20 in.) embedment length samples. Observed and measured responses for other test samples were similar in nature but with different characteristic values and are summarized in the subsequent tables.

Table 4 summarizes the ISO 6891 [1] values for each test, including the mean value and coefficient of variation (COV) for each embedment depth. All tests are labeled with the embedment depth in imperial units followed by a hyphen, followed by a unique number with 2 leading zeros. A COV value below 15 % is desired according to ICC-AC526 and is generally observed. The COV for initial slip and modified initial slip for 304.8 mm (12 in.) embedment, initial slip for 508.0 mm (20 in.) embedment, and reloading elastic slip were above 15 %. For all combinations, including 304.8 mm versus 508 mm, 304.8 mm versus 609.6 mm, and 508 mm versus 609.6 mm, t-tests performed on the monotonic test data showed no statistically significant difference between average stiffness, calculated as the average of all unloading and reloading stiffnesses for one embedment depth, at different embedment depths. Therefore, results indicate there is no apparent relation between embedment depth and stiffness. However, a significant positive relationship between peak load and displacement at peak load was apparent, with initial slip and modified initial slip also following this relationship. Using the mean and COV values listed in Table 4, the fifth percentile of peak loads was determined assuming a normal distribution. The fifth percentiles of peak load were 130.8 kN (29.4 kips), 225.5 kN (50.7 kips), and 237.5 kN (53.4 kips) for the 304.8 mm (12 in.), 508.0 mm (20 in.), and 609.6 mm (24 in.) embedment depths, respectively. Because only one (1) monotonic test was performed at the 812.8 mm (32 in.) embedment, the fifth percentile value is not reported.

Table 5 summarizes the test results according to ICC-AC526 for each embedment depth. The nominal GIR strength is the average peak load for each embedment depth, and the allowable GIR strength is the nominal GIR strength divided by 5. The displacement at allowable GIR load decreases for the 812.8 mm (32 in.) embedment, despite an increase for the three (3) shorter embedments, which indicates that further testing of the 812.8 mm (32 in.) embedment is needed. Nevertheless, the displacement of the 812.8 mm (32 in.) embedment at allowable and ultimate strengths was quite small.

Table 6 lists the cyclic test results for each embedment depth, including peak load, number of cycles to reach the peak load, and cyclic elastic stiffness. Test 12–002 displayed a lower number of cycles to peak load and a reduced elastic stiffness, resulting in a COV over 15 %. All other tests remained within acceptable COV limits (i.e., less than 15 %). The cyclic elastic stiffness for 508.0 mm (20 in.) embedment was only 0.2 % greater, and it was deemed further testing was not required. Deeper embedment depths resulted in more consistent strength and stiffness parameters, but only one (1) test was performed for 812.8 mm (32 in.) embedment depth and therefore were not included in statistical analysis. To characterize the relation between embedment depth and stiffness for cyclic tests, unpaired t-tests for all combinations of embedment depth were performed. Comparing the stiffness for the 304.8 mm (12 in.) group to the stiffness of the 508 mm (20 in.) group as well as comparing the stiffness of the 508 mm (20 in.) group to the stiffness of the 609.6 mm (24 in.) group, no statistically significant difference was found between the mean stiffness. However, comparing the stiffness for the 304.8 mm (12 in.) group and 609.6 mm (24 in.) group, results show a p-value of 0.0327, which indicate there is a statistically significant difference between the mean values for these two groups. The mixed results indicate that that further cyclic testing is required to draw definitive conclusions on the relation between embedment depth and cyclic elastic stiffness of the connection.

Table 7 lists the mean peak load for monotonic and cyclic tests at each embedment depth. An increase in peak load was observed for the 304.8 mm (12 in.) embedment depth. For other embedment depths, a negligible difference in load was noted. Again, for the 812.8 mm (32 in.) embedment depth, only one (1) test was performed for each of monotonic and cyclic loading.

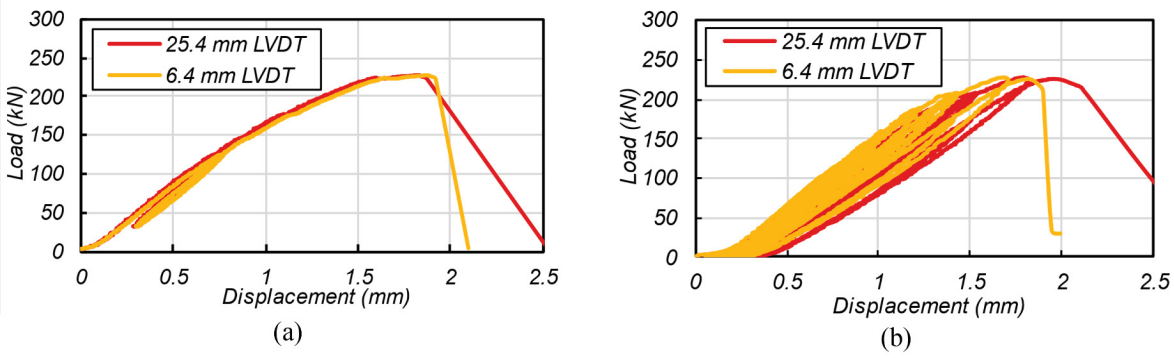

Fig. 6. Example load versus displacement graph of (a) monotonic test and (b) cyclic test.

Table 4
Summary of monotonic tension test results.

D (mm)	Test (D - #)	PL (kN)	DPL (mm)	IS (mm)	MIS (mm)	ESU (kN/mm)	ESR (kN/mm)
304.8	12–001	158.7	1.17	0.71	0.46	234.7	221.7
	12–005	133.5	1.52	0.89	0.41	200.7	195.6
	12–006	157.1	1.22	0.46	0.61	193.3	194.7
	Mean	**149.8**	**1.30**	**0.69**	**0.48**	**209.6**	**204.0**
	COV	*7.7 %*	*12.0 %*	*25.8 %*	*17.6 %*	*8.6 %*	*6.1 %*
508.0	20–001	227.5	1.85	0.74	0.79	204.9	290.9
	20–005	226.7	1.93	0.66	0.71	185.6	188.1
	20–006	230.3	2.29	1.04	0.64	213.3	214.9
	Mean	**228.2**	**2.03**	**0.81**	**0.71**	**201.2**	**231.3**
	COV	*0.7 %*	*9.3 %*	*20.3 %*	*8.7 %*	*5.8 %*	*18.8 %*
609.6	24–001	268.2	2.79	1.01	1.01	186.0	187.7
	24–005	252.3	2.79	1.01	0.89	192.1	196.3
	24–006	243.2	2.54	1.01	0.81	213.0	212.6
	Mean	**254.6**	**2.72**	**1.01**	**0.91**	**197.0**	**198.9**
	COV	*4.1 %*	*4.4 %*	*0.0 %*	*9.3 %*	*5.9 %*	*5.2 %*
812.8	32–001	292.8	3.56	0.79	0.86	195.6	196.1

Peak load (PL), displacement at peak load (DPL), initial slip (IS), Modified initial slip (MIS), elastic stiffness of unloading (ESU), and elastic stiffness of reloading (ESR) for all embedment depths (D).

Table 5
Summary of values reported according to ICC-AC526 (2021).

D (mm)	NGS (kN)	AGS (kN)	AGS_{LFRD} (kN)	DA (mm)	ADL (mm)	DUL (mm)	LUL (mm)
304.8	149.8	29.9	64.6	0.36	2.11	1.30	25.4
508.0	228.2	45.6	98.5	0.53	2.11	2.03	25.4
609.6	254.6	50.9	109.9	0.64	2.11	2.72	25.4
812.8	292.8	58.6	126.4	0.43	2.11	3.56	25.4

Nominal GIR strength (NGS), allowable GIR strength (AGS), allowable GIR strength in LRFD (AGS_{LRFD}), displacement limit at allowable GIR strength (DA), allowable displacement limit per ICC-AC526 (ADL), displacement limit at ultimate loads (DUL), and limit for ultimate displacement limit per ICC-AC526 (LUL) for all embedment depths (D).

Table 6
Summary of cyclic testing results.

Embedment Depth (mm)	Test ID	Peak Load (kN)	Number of Cycles to Peak Load	Cyclic Elastic Stiffness (kN/mm)
304.8	12–002	143.3	14	79.2
	12–003	162.8	26	142.6
	12–004	167.2	26	104.6
	Mean	**157.8**	**22**	**108.8**
	COV	*8.1 %*	*31.5 %*	*24.0 %*
508.0	20–002	227.8	23	154.3
	20–003	223.1	20	158.8
	20–004	224.1	20	213.1
	Mean	**225.0**	**21**	**175.5**
	COV	*1.1 %*	*8.2 %*	*15.2 %*
609.6	24–002	240.8	17	166.7
	24–003	249.7	20	163.6
	24–004	239.9	17	179.3
	Mean	**243.5**	**18**	**169.9**
	COV	*2.2 %*	*9.6 %*	*4.0 %*
812.8	32–002	276.6	20	151.8

Table 7
Difference between monotonic and cyclic loadings.

Embedment Depth (mm)	Mean Peak Load from Monotonic Tests (kN)	Mean Peak Load from Cyclic Tests (kN)	Difference (%)
304.8	149.8	157.8	5.35
508.0	228.2	225.0	−1.40
609.6	254.6	243.5	−4.36
812.8	292.8	276.6	−5.53

Recall that Equation (1), listed in Table 1, considers factors for moisture, rod type, and adhesive type. A modified k_e factor was developed for the tested wood-adhesive combination reported in this paper. Fig. 7 plots the mean peak load using ISO 6891 [1] nominal GIR strength and the full dataset for standard deviation alongside estima1ted capacities using $k_e = 1$ and a modified $k_e = 0.65$. Additionally, the nominal yield and ultimate strength of the ASTM F1554 Grade 105 rods are overlayed for comparison. This calibration was only carried out for the experimental adjustment of the ultimate tensile capacity of the connection versus the embedment length of the rod, since other factors in the equation, k_m and k_b, do not require calibration because the bar type and moisture content correspond directly to the range of values provided in [11]. All other variables are attributed to the geometry of the connection.

4. Discussion

Clear trends arise in the data reported in the Results section. First, the relationship between embedment depth and tensile capacity was concave, and therefore, not linear. In contrast, there was no apparent trend for mean elastic stiffness for the unloading and reloading phase of each embedment depth, as shown in Table 4. The mean stiffness of all unloading and reloading phases across embedment depths was 205.4 kN/mm (1173 kip/in) with a COV of 3.5 %. The mean stiffness for cyclic testing across all embedment depths was 151.4 kN/mm (864.5 kip/in) with a COV of 23.4 %. Unpaired t-tests were performed on these data and determined that there was a statistically significant difference between the monotonic and cyclic test results. However, the high COV for cyclic testing suggests that further testing should be performed to better characterize this relation. Lastly, displacements were small and below the allowable displacement limit specified in ICC-AC526.

A comparison between monotonic and cyclic testing capacities shows a minimal loss in tensile capacity following multiple load cycles. Unpaired, two-tailed t-tests were performed to assess the significance of the difference in means between monotonic and cyclic load testing. Table 8 summarizes data from these tests, where no significant difference was found for any of the three (3) embedment depths (*t*-test on 812.8 mm embedment depth could not be performed because only a single data point was taken for each testing protocol). A level of significance of 0.10 for rejecting the null hypothesis was used to account for the small sample size. While results show that the difference was not significant for all testing, a larger sample size would be necessary to confirm this outcome.

For all samples, failure occurred at the bond interface between the adhesive and MPP. Fig. 8 shows typical failure conditions. Fig. 8b shows

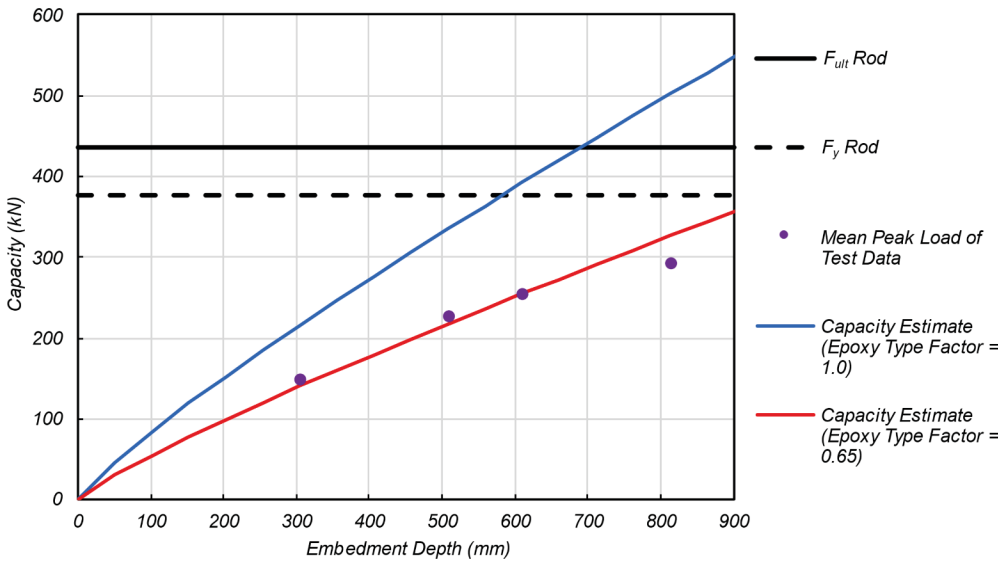

Fig. 7. Tensile capacity versus embedment depth for ISO 6891 [1] test results (circles) along with estimates using Deng's equation with an adhesive type factor of 1 and 0.65.

Table 8
Tension capacities for monotonic and cyclic load testing and summary of *t*-test results difference in means between monotonic and cyclic load testing tension capacity results.

Embedment Depth (mm)	Mean (kN)		Standard Deviation (kN)		T-value	p-value
	Monotonic	Cyclic	Monotonic	Cyclic		
304.8	149.8	157.8	14.1	12.72	0.73	0.506
508.0	228.2	225.0	1.9	2.5	1.76	0.153
609.6	254.6	243.5	12.7	5.4	1.40	0.235

an example where it is seen that the placement of the rods was not concentric within the predrilled holes for all samples. However, there was no observable change in tensile capacity for these conditions. Additionally, other literature has resulted in load versus displacement responses that were more ductile, but because the steel tensile capacity was larger than the failure load and the edge distance was greater than the minimum suggestions, failure near the wood and adhesive interface controlled for all specimens [25,21,4,5]. Parida et al. [19]. This suggests that explicit detailing can result in a ductile connection instead of the brittle failure shown here. This detailing requires ensuring that the yielding of the rod occurs prior to the failure of the glue line.

Two (2) failure conditions were exhibited in the tested samples. First, splitting of the MPP occurred for some samples. This splitting would extend between 25 % and 50 % of the clear spacing between two rods, but none reached other samples. Fig. 9a shows the splitting that occurred in the cross-section located at halfway down the embedment depth (specimen with 508.0 mm (20 in.) embedment shown). However, because the HSS parts of the testing fixture cover the edge of the MPP adjacent to the rod, determining initiation of splitting during loading was not possible. The second failure mode observed was pullout of an

Fig. 8. Observed failure near the load application: (a) wood failure for concentric rod placement, and (b) impact of a rod aligned against drilled hole.

Fig. 9. (a) Splitting of MPP and (b) separation at adhesive-wood intersection. Sections taken at one-half of specimen embedment depth (254 mm for shown specimen).

adhesive plug with wood fibers from the MPP. Fig. 9b shows this failure mode.

In all samples, "popping" sounds would occur during the initial loading period where the initial slip was calculated and on the first cycle during cyclic testing, occurring between 30 % and 50 % of the peak load for each test. There was no change observed in the slope of the load-deformation response when "popping" occurred. However, near failure (60 %-80 % of peak load), the "popping" would return until a large "pop" coinciding with failure of the samples and a large drop in load.

One problem found post testing was that in one of the samples (Test 12–005), the adhesive was not fully cured. The uncured adhesive portion was roughly 30 % of the entire area, resulting in a peak load drop of 16 %. Note that this lack of curing was only observed for a single specimen.

5. Conclusions

Experiments were conducted to assess the tensile capacity and stiffness of individual glued-in rods bonded into Mass Ply Panels. Two (2) different loading protocols were considered and four (4) different embedment depths were investigated. From the measured test results, key response characteristics were established, and existing analytical predictions were calibrated to the data. Based on this study, the following conclusions are presented.

1. The nominal and allowable strength of the glued-in rod (GIR) for different embedment depths were determined and shown in Table 5. These values can help designers utilize this connection in practice. However, further work characterizing multiple GIR connections is needed.
2. The monotonic elastic stiffness of the connection was not correlated to embedment depth. This finding is supported by Azinovic et al. [21], which concluded that the global stiffness of GIR connections mostly depends on the rod diameter. For the test performed herein, results indicate that the mean monotonic elastic stiffness was 205.4 kN/mm (1173 kip/in). Further cyclic testing is required to determine the relationship between cyclic elastic stiffness and both embedment depth and monotonic elastic stiffness.
3. Test results from the ISO 6891 [1] and cyclic loading protocols showed no statistical difference in tensile capacity according to t-tests. This indicates that the simpler monotonic test protocol can be used for cyclic strength characterization for the variables and conditions considered.
4. To quantify tensile capacity for all embedment depths between 304.8 mm (12 in.) and 812.8 mm (32 in.), a wood adhesive type factor,k_e, for use with Deng's equation in Table 1 was derived using regression of the ISO 6891 [1] testing values (purple circles in Fig. 7). A factor of $k_e = 0.65$ was found to fit well to the data for this adhesive and timber layup combination. Note that this k_e is only valid for the specific adhesive-timber combination evaluated (i.e., MPP and Simpson CI-GV epoxy gel). However, the specimen fabrication and testing protocols developed in this paper are applicable to any combination of adhesive and timber.

The GIR connection shows promise for use as an embedded splice connection for mass timber shear walls. However, this study considered only a single connection combination with one substrate, one adhesive, one anchor rod, and one connection geometry and future work should include testing of other connection combinations. Additionally, although an edge distance less than 2.5d was provided, alternating screws were added to mitigate the MPP splitting as a primary failure mode. With sufficient additional data, a predictive equation could eventually be developed for multiple combinations of timber species, layup, rod type, adhesive type, and geometry. This data is available for smaller diameters and embedment depths but lacking for large connection configurations required in contemporary designs. Additional testing is needed for GIR connections with longer embedment depths, larger rod diameters, group actions, and under cyclic loading.

CRediT authorship contribution statement

Tanner Field: Writing – review & editing, Writing – original draft, Investigation, Formal analysis. **Andre R. Barbosa:** Writing – review & editing, Writing – original draft, Validation, Supervision, Project administration, Methodology, Investigation, Funding acquisition, Data curation, Conceptualization. **Reid B. Zimmerman:** Writing – review & editing, Methodology, Conceptualization. **Steve Pryor:** Writing – review & editing, Methodology, Conceptualization. **Arijit Sinha:** Writing – review & editing. **Christopher Higgins:** Writing – review & editing.

Declaration of Competing Interest

The authors declare that they have no known competing financial interests or personal relationships that could have appeared to influence the work reported in this paper.

Data availability

Data will be made available on request.

Acknowledgments

The authors would like to acknowledge the assistance of Tyler Deboodt in conducting the laboratory tests and Phil Mann for help preparing the test specimens. This study was performed to support the design of the 10-story and 6-story NHERI TallWood Design projects. Financial support was provided by the TallWood Design Institute with funding from the U.S. Department of Agriculture's Agricultural Research Service (USDA ARS) Agreement No. 58-0204-9-165, National Science Foundation award number 2120683, and by in-kind support from Simpson Strong-Tie. The findings and conclusions in the manuscript are the responsibility of the authors and do not necessarily reflect the sponsors or those acknowledged.

References

[1] International Organization for Standardization. (1983). Occupational Health and Safety Management Systems—Requirements with Guidance for Use (ISO Standard No. 6891:1983). https://www.iso.org/standard/13413.html.
[2] G. Tlustochowicz, E. Serrano, R. Steiger, State-of-the-art review on timber connections with glued-in steel rods, Mater. Struct. 44 (5) (2010) 997–1020, https://doi.org/10.1617/s11527-010-9682-9.
[3] E. Gonzalez, C. Avez, T. Tannert, Timber joints with multiple glued-in steel rods, J. Adhes. 92 (7–9) (2015) 635–651, https://doi.org/10.1080/00218464.2015.1099098.
[4] B. Azinović, H. Danielsson, E. Serrano, M. Kramar, Glued-in rods in cross laminated timber – numerical simulations and parametric studies, Constr. Build. Mater. 212 (2019) 431–441, https://doi.org/10.1016/j.conbuildmat.2019.03.331.
[5] C. Grunwald, T. Vallée, S. Fecht, O. Bletz-Mühldorfer, F. Diehl, L. Bathon, S. Myslicki, R. Scholz, F. Walther, Rods glued in engineered hardwood products part I: experimental results under quasi-static loading, Int. J. Adhes. Adhes. 90 (2019) 163–181, https://doi.org/10.1016/j.ijadhadh.2018.05.003.
[6] G. Muciaccia, An Experimental approach to determine pullout strength of single and multiple axially loaded steel rods bonded in glulam parallel to the grain, Wood Mat. Sci. Eng. 14 (2) (2017) 88–98, https://doi.org/10.1080/17480272.2017.1404491.
[7] M. Sofi, E. Lumantarna, R. Hoult, M. Mooney, N. Mason, J. Lu, Bond strength of GIR in cross-laminated timber: A preliminary study, Constr. Build. Mater. 301 (2021), 123864, https://doi.org/10.1016/j.conbuildmat.2021.123864.
[8] H. Zhang, H. Li, A. Dauletbek, R. Lorenzo, I. Corbi, O. Corbi, Research status of glued-in rod connections in wood structures, J. Build. Eng. 65 (2023), 105782, https://doi.org/10.1016/j.jobe.2022.105782.
[9] P.K. Townsend, Steel Dowels Epoxy Bonded in Glue Laminated Timber. Research Report 90–11, Department of Civil Engineering, University of Canterbury, Christchurch, New Zealand, 1990.
[10] R. Steiger, E. Serrano, M. Stepinac, V. Rajčić, C. O'Neill, D. McPolin, R. Widmann, Strengthening of Timber Structures with Glued-in rods, Constr. Build. Mater. 97 (2015) 90–105.
[11] X. Deng, Strength of the Epoxy Bonded Steel Connection in Glue Laminated Timber: A Thesis Submitted in Partial Fulfilment of the Requirements for the Degree of Doctor of Philosophy in Civil Engineering at the University of Canterbury, Department of Civil Engineering, University of Canterbury, Christchurch, New Zealand, 1997. Doctoral dissertation.
[12] E. Serrano, Glued-in Rods for Timber Structures—A 3D Model and Finite Element Parameter Studies, Int. J. Adhes. Adhes. 21 (2) (2001) 115–127.
[13] D.O. Chans, J.E. Cimadevila, E.M. Gutiérrez, Withdrawal Strength of Threaded Steel Rods Glued with Epoxy in Wood, Int. J. Adhes. Adhes. 44 (2013) 115–121.
[14] CEN (2005a) EN 1995-1-1: Eurocode 5: Design of timber structures Part 1: Common rules and rules for buildings. European Committee for Standardisation.
[15] Y. Yan, H. Liu, X. Zhang, H. Wu, Y. Huang, The effect of depth and diameter of glued-in rods on pullout connection strength of bamboo glulam, J. Wood Sci. 62 (1) (2016) 109–115.
[16] G.S. Ayansola, T. Tannert, T. Vallee, Experimental investigations of glued-in rod connections in CLT, Constr. Build. Mater. 324 (2022), 126680, https://doi.org/10.1016/j.conbuildmat.2022.126680.
[17] Mislav Stepinac, F. Hunger, R. Tomasi, E. Serrano, V. Rajcic, van de Kuilen, J. Willem, Comparison of design rules for glued-in rods and design rule proposal for implementation in european standards, in: Proceedings of CIB-W18, Vancouver, Canada, 2013, pp. 85–99.
[18] V. Wiberg, Single Glued-in-Rod Connections for Timber Structures: A State-of-the-Art Review. Master's dissertation. Department of Architecture and Civil Engineering, Chalmers University of Technology, Gothenburg, Sweden, 2019.
[19] D. Yeboah, S. Taylor, D. McPolin, R. Gilfillan, S. Gilbert, Behaviour of joints with bonded-in steel bars loaded parallel to the grain of timber elements, Constr. Build. Mater. 25 (5) (2011) 2312–2317, https://doi.org/10.1016/j.conbuildmat.2010.11.026.
[20] G. Parida, H. Johnsson, M. Fragiacomo, Provisions for ductile behavior of timber-to-steel connections with multiple glued-in rods, J. Struct. Eng. 139 (9) (2013) 1468–1477, https://doi.org/10.1061/(asce)st.1943-541x.0000735.
[21] B. Azinović, E. Serrano, M. Kramar, T. Pazlar, Experimental investigation of the axial strength of glued-in rods in cross laminated timber, Mater. Struct. 51 (6) (2018), https://doi.org/10.1617/s11527-018-1268-y.
[22] B.-H. Xu, D.-F. Li, Y.-H. Zhao, A. Bouchaïr, Load-carrying capacity of timber joints with multiple glued-in steel rods loaded parallel to grain, Eng. Struct. 225 (2020), 111302, https://doi.org/10.1016/j.engstruct.2020.111302.
[23] J. Thamboo, S. Navaratnam, T. Ponnampalam, Pull-out resistance of glued in Rod Connection in timber: Reliability analyses using an experimental database, Constr. Build. Mater. 344 (2022), 128291, https://doi.org/10.2139/ssrn.4107429.
[24] Krawinkler, H., F. Parisi, L. Ibarra, A. Ayoub, and R. Medina. (2000). Development of a Testing Protocol for Wood Frame Structures. CUREE Publ. No. W-02. Consortium of Universities for Research in Earthquake Engineering. Richmond, California.
[25] B.H. Xu, A. Bouchaïr, M. Taazount, E.J. Vega, Numerical and experimental analyses of multiple-dowel steel-to-timber joints in tension perpendicular to grain, Eng. Struct. 31 (10) (2009) 2357–2367, https://doi.org/10.1016/j.engstruct.2009.05.013.